Published in final edited form as:
Gastroenterology. 2012 September ; 143(3): 589–598.e3. doi:10.1053/j.gastro.2012.05.036.

Abnormal Initiation and Conduction of Slow-Wave Activity in Gastroparesis, Defined by High-Resolution Electrical Mapping

Gregory O'Grady[1,2], **Timothy R. Angeli**[2], **Peng Du**[2], **Chris Lahr**[3], **Wim JEP Lammers**[2,4], **John A. Windsor**[1], **Thomas L. Abell**[3], **Gianrico Farrugia**[5], **Andrew J. Pullan**[2,6,*], and **Leo K. Cheng**[2,6]

[1]Department of Surgery, University of Auckland, New Zealand [2]Auckland Bioengineering Institute, University of Auckland, New Zealand [3]Division of Gastroenterology, University of Mississippi Medical Center [4]Department of Physiology, UAE University, United Arab Emirates [5]Division of Enteric Neurosciences, Mayo Clinic, Rochester, MN, USA [6]Department of Surgery, Vanderbilt University, Nashville, Tennessee, USA

Abstract

Background & Aims—Interstitial cells of Cajal (ICC) generate slow waves. Disrupted ICC networks and gastric dysrhythmias are each associated with gastroparesis. However, there are no data on the initiation and propagation of slow waves in gastroparesis, because research tools have lacked spatial resolution. We applied high-resolution electrical mapping to quantify and classify gastroparesis slow-wave abnormalities in spatiotemporal detail.

Methods—Serosal HR mapping was performed, using flexible arrays (256 electrodes; 36 cm^2), at stimulator implantation in 12 patients with diabetic or idiopathic gastroparesis. Data were analyzed by isochronal mapping, velocity and amplitude field mapping, and propagation animation. ICC numbers were determined from gastric biopsies.

Results—Mean ICC counts were reduced in patients with gastroparesis (2.3 vs 5.4 bodies/field; $P<.001$). Slow-wave abnormalities were detected by HR mapping in 11/12 patients. Several new patterns were observed and classified as 'abnormal initiation' (10/12; stable ectopic pacemakers or diffuse focal events; median 3.3 c/min, range 2.1-5.7), or 'abnormal conduction' (7/10; reduced velocities or conduction blocks; median 2.9 c/min; range 2.1-3.6). Circumferential conduction emerged during aberrant initiation or incomplete block and was associated with velocity elevation (7.3 vs 2.9 mm s^{-1}; $P=.002$) and increased amplitudes beyond a low base value (415 vs 170 μV; $P=.002$).

Corresponding author: Dr Gregory O'Grady, Department of Surgery, Faculty of Medical and Health Sciences, University of Auckland, Private Bag 92019, Auckland, New Zealand, Phone: 0064-21-448-523; Fax: 0064-9-377-9656, gog@ps.gen.nz.
*Deceased; March 2012

Disclosures:
GOG, PD, AJP and LKC hold intellectual property in GI multi-electrode mapping. TLA is a Licensor, Consultant, Investigator for Medtronic, Inc.

Author Contributions:
Conception and design: GOG, CL, GF, TLA, AJP, LKC. Data collection: GOG, TRA, PD, CL, GF, TLA, AJP, LKC. Analysis/ Interpretation of Data: GOG, TRA, PD, WJEPL, JAW, GF, AJP, LKC. Drafting of article: GOG; Critical revisions: TRA, PD, WJEPL, JAW, GF, TLA, LKC. Final approval of article: All authors.

Conclusions—HR mapping revealed new categories of abnormal human slow-wave activity. Abnormalities of slow-wave initiation and conduction occur in gastroparesis, often at normal frequency, which could be missed by tests that lack spatial resolution. Irregular initiation, aberrant conduction, and low amplitude activity could contribute to the pathogenesis of gastroparesis.

Keywords

Bradygastria; tachygastria; gastric electrical activity; electrogastrography

Introduction

Among several mechanisms contributing to the pathophysiology of gastroparesis, the role of the interstitial cells of Cajal (ICC) is receiving increased attention [1]. Recent studies have shown that ICC abnormalities are the most pronounced cellular defects in both diabetic and idiopathic gastroparesis [2,3]. In a recent electron microscopy study, ICC abnormalities were found in 40/40 patients with idiopathic or diabetic gastroparesis [3]. ICC generate and propagate the slow-wave activity that coordinates gastric peristalsis [4], and dysrhythmic slow-wave activity has been described in animal models [5] and patients with gastroparesis in several studies [6,7,8].

Despite the prominence of these associations, the specific slow-wave abnormalities occurring in human gastroparesis remain poorly defined. Previous studies have applied cutaneous electrogastrography (EGG) and sparse serosal or mucosal electrode recordings to define deviations in slow-wave frequency and rhythm [9,10]. However, owing to their lack of spatial resolution, these tests cannot yet reliably quantify and classify abnormal slow-wave initiation and conduction [11,12]. As ICC loss occurs throughout the stomach in gastroparesis [2,5], useful evaluations of slow-wave propagation may depend on adequate spatial resolution.

High-resolution (HR) electrical mapping has recently been advanced as an improved technique for evaluating abnormal slow-wave activity [11,12]. As in cardiac electrophysiology, HR mapping involves the positioning of spatially-dense arrays of electrodes on the organ surface to permit the recording and reconstruction of patterns of electrical activation in spatiotemporal detail. Recent animal model HR mapping studies have revealed significant new insights concerning the patterns and mechanisms of gastric slow-wave dysrhythmias [11,12].

In this study, we applied HR mapping to evaluate slow-wave abnormalities occurring in patients with diabetic and idiopathic gastroparesis. We hypothesized that abnormalities of both slow-wave initiation and conduction occur in gastroparesis, and this study aimed to define, quantify and classify these abnormalities in fine spatiotemporal detail.

Methods

Ethical approval for this work was granted by the University of Mississippi Medical Center (UMMC) and the Mayo Clinic Institutional Review Boards. Consecutive patients with medically-refractory gastroparesis, confirmed by standardized scintigraphy protocol testing (≥10% meal retention at 4 hours) [13], who were undergoing gastric electrical stimulator implantation at UMMC, were invited for inclusion. Patients with malignancy, primary eating disorders or pregnancy were excluded.

Demographic data, disease aetiology, medical histories, and BMI were recorded for each patient. 'Total symptom scores' (TSS) were calculated by scoring five symptoms (pain,

bloating/distension, nausea, vomiting, and early satiety) on a 5-point Likert scale: 0 = absent, 1 = mild (not influencing usual activities), 2 = moderate (causing diversions from usual activities), 3 = severe (urging modification of usual activities), 4 = extremely severe (markedly restricting usual activities).

Experimental Protocol

All experiments were performed in the operating room following general anesthesia and upper midline laparotomy. Slow-wave activity has been reliably recorded under anesthesia in other studies [14,15], and the anesthetic methods in this investigation were similar to those used in another recent intra-operative mapping study of 12 normal human subjects [16], all of whom showed consistently normal slow-wave activity. The anaesthetic regimen used in these patients is provided in Suppl. Table 1.

HR mapping was performed using flexible printed circuit board (PCB) arrays [17]. Each PCB had 0.3 mm diameter electrode contacts, with 32 electrodes in a 16 × 2 configuration at a 4 mm inter-electrode spacing. Eight PCBs were aligned and joined with a sterile adhesive and used simultaneously (256 electrodes total; 16 × 16 array; 36 cm^2) (Figure 1A). Mapping was undertaken immediately after laparotomy and prior to organ handling or stimulator placement. The PCBs were laid on the anterior serosa of the stomach; the posterior surface was not mapped (Figure 1B). Mapped positions were defined with reference to anatomical landmarks, as previously described [16]. Warm saline-soaked gauze was laid over the PCBs, the wound edges were approximated, and the cables were attached loosely to a retractor, such that they could move freely with respiratory excursion (Figure 1C). The recording period was approximately 15 minutes in each case, with two or three adjacent gastric areas being mapped per patient.

At recording, reference electrodes were placed on the shoulders and raw (unfiltered) unipolar signals were acquired at 512 Hz using a modified Active Two System (Biosemi, The Netherlands). Each PCB was connected to the ActiveTwo via a sterilized 1.5 m 68-way ribbon cable, and the ActiveTwo was fibre-optically connected to a laptop. Acquisition software was written in Labview v8.2 (National Instruments, TX).

ICC Histology

Full-thickness gastric biopsies were taken from the anterior stomach, midway between the curvatures and 9 cm proximal to the pylorus, in 9/12 patients. Age and sex-matched control specimens were collected from the same location in patients undergoing gastric bypass surgery, who were free of gastrointestinal diseases or diabetes. Obesity has been shown not to affect ICC numbers [2]. ICC cell bodies in the circular muscle layer were identified using a Kit antibody (Lab Vision MS-483-P, mouse 1:400) and a 4′,6-diamidino-2-phenylindole (DAPI) nucleus counter-stain, and were quantified as bodies per field according to the methods described by Grover et al [2].

Signal Processing

HR mapping analysis was performed with the Gastrointestinal Electrical Mapping Suite (GEMS) (v1.3) [18]. Recordings were down-sampled to 30 Hz, and filtered with a moving median filter for baseline correction and a Savitzky-Golay filter for high-frequency noise [19]. Slow-wave activation times were identified using the FEVT algorithm [20], and clustered into discrete wavefronts (cycles) using the REGROUPS algorithm [21] (Figure 1D), with thorough manual review and correction of all results. Activation maps were calculated [21] (Figure 1E), and sites of conduction block (cessation of a propagating wavefront) were automatically corrected when required [22]. Animations were generated for the analyzed data segments, with periods of normal activity colored blue, and abnormal activity colored red.

Frequency was determined by averaging the cycle intervals at all electrodes. Velocity vector fields were calculated using a finite difference approach, with interpolation and Gaussian filter smoothing, and visualized by overlaying arrows showing propagation direction on a 'speed map' (Figure 1E) [23]. Amplitudes were calculated by using a peak-trough detection algorithm based on the 'zero-crossing' of the first and second-order signal derivatives of each event, and visualized by assigning a color gradient according to magnitude (Figure 1E) [19]. Corpus results (which show consistent velocities and amplitudes in normal circumstances [16]) were decomposed into longitudinal and circumferential components for comparison as previously described [24].

Interpretation and Analysis

Normal reference data were previously established using similar HR mapping methods in 12 patients with normal stomachs, who were undergoing mainly pancreatic or hepatic resections for neoplastic disease [16]. This previous normal cohort consisted of 7 males, and 5 females, of median age 50 yrs (range 21-60) (Suppl. Table 1). All data were screened for deviations from normal activity by isochronal mapping and animation, and abnormalities were identified and quantified by frequency, rhythm (regular vs irregular), and spatial pattern [12]. Tachygastria was defined as ≥3.7 c/min and bradygastria as ≤2.4 c/min, based on one commonly cited normal range [9,10]. Mean or median values are given together with standard deviations (SD) or standard error of the mean (SEM). Student's t-test was used for the statistical analyses (threshold $p<0.05$), and 95% confidence intervals (CI) are reported.

Results

Study Population

HR gastric mapping was performed on a consecutive cohort of 12 patients with gastroparesis, six male and six female, with eight having a diabetic and four an idiopathic etiology. The median age was 42 yrs (range: 30 – 62), median 4-hr gastric retention was 26% (range: 14 – 75%), median TSS was 16/20 (range: 13 – 20) and median BMI was 27 (range: 15.5 – 46). Individual patient data are reported in Suppl. Table 2. The mean glycosylated haemoglobin (HbA_{1c}) was 6.7 (S.D 1.3), and the mean perioperative blood glucose level was 7.4 (S.D 2.4) mmol/l.

ICC Counts

Mean ICC counts were available and analyzed for 9/12 patients, and were compared to ICC counts from the matched controls (mean age difference 0.5 ± 0.7 SD yrs; sex identical). ICC counts were substantially reduced in gastroparesis patients as compared to those of the matched controls, at (2.3 ± 0.3 SEM vs 5.4 ± 0.4 SEM) bodies/field; $P<0.0001$) (Figure 2). Tissue sections were also labelled with DAPI to identify nuclei. No difference in total number of nuclei in the muscle layers was noted between controls and gastroparesis suggesting that there was no difference in stretch between the 2 groups (100 ± 7 SEM nuclei/field in controls vs 103 ± 5 SEM in diabetic gastroparesis vs 99 ± 7 SEM in idiopathic gastroparesis). Individual patient ICC counts are reported in Suppl. Table 2.

HR Propagation Analysis

All patients underwent a continuous period of mapping after the abdomen was opened, but before manipulation of any organs, for a mean duration of 13.4 (SD 4.6) min/patient. Abnormal slow-wave activity was recorded in 11/12 patients, and ranged from minor transient deviations from normal slow-wave activity to persistent and highly disorganized patterns. The abnormalities were classified into either abnormalities of initiation (10/12 patients), or abnormalities of conduction (7/12), which often co-existed (7/12), and then sub-

classified by pattern, rhythm and rate according to the scheme developed in Figure 3. No difference was observed in dysrhythmia patterns between the diabetic and idiopathic subgroups (Figure 3), hence these groups are reported together in this study.

The median slow-wave frequency across the cohort was 3.1 c/min (range: 2.1 – 5.7), and 7/12 patients had normal frequencies throughout their recordings. However, as detailed below, normality of frequency did not imply normal propagation patterns, because both initiation and conduction abnormalities routinely occurred at normal frequencies (Figure 3).

One patient (ID#3 in Suppl. Table 2) showed exclusively normal slow-wave propagation at a normal frequency throughout the recording despite a reduced ICC count (1.7 ± 1.5 SD bodies/field). Continuous normal slow-wave propagation was also observed in a second patient with a reduced ICC count (ID#8; 2.0 ± 1.6 SD bodies/field), although at a modestly increased frequency (mean 3.9 ± 0.3 SD c/min).

Abnormalities of slow-wave initiation—Aberrant (ectopic) slow-wave initiation occurred in 10/12 patients and was the most common class of abnormality. An abnormal initiation was classified as either regular (corresponding to a stable site of ectopic pacemaking; 7/10 patients), or irregular, (corresponding with ectopic focal events arising at variable locations across the mapped field (5/10) (Figure 3). In two patients, regular and irregular patterns of abnormal initiation were observed at separate instances of time within the same recording period.

Figure 4, Suppl. Figure 1, and Figure 5, and accompanying animations, show examples of abnormal initiation patterns, representative of the categories shown in Figure 3. Figure 4 details the slow-wave patterns underlying unstable focal events and stable ectopic pacemaking at high frequency (irregular and regular tachygastria). Suppl. Figure 1 details stable and unstable ectopic patterns occurring in adjacent uncoupled regions of the same stomach, at mismatched frequencies. Figure 5 details examples of stable ectopic pacemaking and unstable focal events occurring at bradygastric frequencies.

Abnormal slow-wave initiation occurred across a wide range of frequencies in both the antrum (median 3.9, range: 2.2 – 5.7 c/min; Figures 4,5) and corpus (median 3.0, range: 2.1 – 4.7 c/min; Figure 5 and Suppl. Figure 1), (mean difference 0.9 c/min, [CI: −0.5, 2.1]). In 5/10 patients, abnormal initiation occurred at normal frequencies. Tachygastria (defined above) was observed in three patients (range: 3.9 – 5.7 c/min) (Figure 4 and Suppl. Figure 1), and bradygastria in three patients (range: 2 – 2.4 c/min) (Figure 5). Abnormal initiation was observed to be transient, occurring before or after a period of normal wavefronts, in 3/10 (Figures 4,5), or persistent, being present for 100% the recorded duration, in 7/10 (Suppl. Figure 1). When abnormal slow-wave initiation was transient, it occurred for mean 51% ± 27% SD of the recorded duration.

During normal cycles, wavefronts were oriented orthogonally to the gastric curvatures and propagated in the longitudinal organ axis (Figure 1E), at a mean corpus velocity of 2.9 ± 0.2 SEM mm s^{-1}, and with mean amplitude 170 ± 25 SEM μV. During aberrant initiation, ectopic activations occurring within a field of resting tissue allowed excitation to progress in all directions, inducing circumferential propagation in all cases (e.g. Figures 4,5). Across all cases, compared to longitudinal conduction, circumferential conduction occurred with a higher mean velocity (7.3 ± 0.9 SEM mm s^{-1} vs 2.9 ± 0.2 SEM mm s^{-1}; P=0.002), as well as a higher mean amplitude (415 ± 65 SEM μV vs 170 ± 25 SEM μV; P=0.002).

Spatial organization and coupling across the mapped field was variable during initiation abnormalities. Spatial uncoupling and colliding wavefronts were more commonly associated

with unstable focal activities than stable ectopic pacemaking (7/10 patients, Fisher's exact test P=0.03, Figures 4,5). Retrograde propagation involving >25% of the mapped field occurred persistently or transiently in most cases (8/10), and was most prominent when abnormal initiation occurred distally (Figure 4,5 and Suppl. Figure 1). Figure 4 demonstrates how chaotic tissue activation during unstable activities could result in a broad range of frequencies across the mapped field.

Abnormalities of Slow-wave Conduction—Abnormalities in slow-wave conduction, were observed in 7/12 patients, all of whom also showed abnormalities of initiation (Figure 3). Abnormalities of conduction were classified as either conduction blocks, representing premature termination of part or all of a propagating wavefront [12] (6/7), or abnormal velocity, representing a regional reduction in the normal longitudinal propagation velocity to 3 SD below the normal range [16] (4/7).

Figure 6 and Suppl. Figure 2, together with accompanying animations, present representative examples of abnormal conduction patterns representative of the categories shown in Figure 3. Figure 6A-B details reduced longitudinal conduction velocity in association with an abnormally narrow spacing between consecutive wavefronts. Figure 6C-F details reduced velocity in association with intermittent incomplete conduction block, as well as the adjacent emergence of aberrant initiation events, often in conjunction with conduction delays (interpreted as 'escape activities' [12]; see Figure 3). Suppl. Figure 2 details a stable and persistent conduction abnormality, of a highly deranged pattern, in a patient with a severely reduced ICC count (0.3 ± 0.6 SD bodies/field).

The median slow-wave frequency in the mapped areas that showed conduction abnormalities was 2.9 (range 2.1 – 3.6) c/min. Abnormal conduction could occur in both the corpus (4/7) and the antrum (3/7). The degree of ICC loss was similar between patients with or without conduction abnormalities (mean 2.2 ±0.6 SEM vs 2.4 ± 0.3 SEM cell bodies/field; P=0.24).

Discussion

This study is the first to apply high-resolution (HR) electrical mapping to quantify human gastric slow-wave abnormalities in spatial detail. The findings present several novel insights into the electrical abnormalities occurring in gastroparesis, and facilitate a newly proposed classification scheme for human gastric electrical disorders.

These findings extend but also challenge current concepts of gastric slow-wave dysrhythmias. Past human dysrhythmia studies have predominantly addressed frequency, because EGG analyses have prioritized the frequency domain [9,25]. However, this study indicates that frequency analysis alone is insufficient in detecting and describing slow-wave abnormalities in gastroparesis. Abnormal activation patterns routinely occurred at normal frequency, and even highly disordered slow-wave patterns could occur at normal frequency and with regular rhythm. Such abnormalities would have gone undetected by methods lacking spatial resolution.

Previous interpretations of human gastric dysrhythmia have focused mainly on abnormalities of slow-wave initiation [9,10,26]. Bradyarrhythmias are thought to result from a failure of normal entrainment, and tachyarrhythmias from the emergence of unifocal ectopic pacemakers or diffuse focal events, often in the antrum, that over-ride the normal frequency gradient [9,10,26]. This study supports these concepts through spatial resolution, but also reveals a greater than expected complexity. The corpus may be a common source of ectopic events across a range of frequencies. Spatial coupling can be highly variable during

initiation abnormalities, with retrograde propagation, wave collisions and uncoupling being more pronounced when initiation sites are more distal, diffuse, or irregular. During unstable focal events, chaotic tissue activation and colliding wavefronts induce an irregular range of frequencies across the stomach, likely explaining the 'tachybradyarrhythmia' pattern previously observed in sparse electrode studies [8,26].

The mechanisms underlying abnormalities of slow-wave initiation in gastroparesis are poorly understood. Metabolic disturbances occurring in diabetics are known to be arrhythmogenic, particularly hyperglycemia [27]. However, additional factors must also contribute, because the patients in this study were euglycemic, and abnormal initiation also occurred in idiopathic patients (as previously reported [8]). Greater degrees of ICC loss have been correlated with higher dysrhythmia rates by EGG [6], suggesting that ICC network impairment predisposes to initiation abnormalities. However, the reasons for this association remain unclear, and the factors inciting episodes of instability need further research. For example, other cell types can influence the slow-wave including enteric nerves that may also be altered in gastroparesis [2].

The first detailed description of human gastric slow-wave conduction abnormalities was a major outcome of this study. Conduction abnormalities have received inadequate attention to date, because spatial resolution is required for their detection [11,12]. Conduction abnormalities likely reflect pathological cell and tissue changes occurring in gastroparesis [2,3], implying that structural defects play a key role in myoelectrical disturbances. It is unlikely that these abnormalities were 'functional' (occurring in anatomically normal tissue), because they were stable and persistent, whereas the functional conduction abnormalities previously described in healthy animal stomachs were exclusively transient (preceded or followed by normal wavefronts) [11,12].

In this study, we chose to focus on ICC, because ICC abnormalities are the predominant cellular defect in gastroparesis and the number of ICC correlates with gastric emptying [2,3,28]. Biophysically-based models have predicted that reduced velocities would result from ICC depletion, due to haphazard conduction at fine tissue scales [29], a hypothesis supported from data in this study. However, more research is required to understand why conduction abnormalities were only prominent in certain gastric regions and patients. This may be because ICC loss in gastroparesis is heterogeneous [2], and conduction defects might reflect localized ICC loss passing a critical threshold. Degradation of remaining ICC is also significant in gastroparesis [2,3], and the degree of functional impairment of these cells may also prove important. Recent ultrastructural studies have also revealed significant fibrosis in the connective stroma of the gastroparetic stomach, particularly in idiopathic cases [3]. Collagen is electrically insulating, and in cardiac mapping, is known to impede conduction, induce propagation delay and promote arrhythmias [30]. A role for fibrosis in gastric conduction defects should therefore be investigated.

Slow-wave re-entry was recently shown to be an important conduction abnormality underlying tachygastria in large animal models [11,12]. Re-entry was not observed in this study, however, abnormalities capable of initiating slow-wave re-entry were prominent, notably focal activities and incomplete conduction blocks [11,12]. Possibly, re-entry could have been detected if a wider area of the stomach had been mapped.

This study also showed for the first time that rapid circumferential conduction is a common feature of human gastric dysrhythmias. Circumferential conduction emerges during dysrhythmia because transverse excitation is enabled by the absence or impairment of the normal ring wavefronts. Velocities and amplitudes were ~2.5× higher during circumferential conduction: a marked difference that offers a new biomarker for detecting dysrhythmic

patterns, which may prove particularly useful when employing small targeted devices [31,32]. The velocity increase may reflect different conduction rates through ICC layers [33], or possibly gap junction distribution differences, while the amplitude rise obeys proportionality between velocity and transmembrane current passing extracellularly [34]. Rapid circumferential conduction has the effect of quickly restoring ring wavefronts during dysrhythmia, therefore, possibly being a beneficial adaptation. On the other hand, once these circumferential wavefronts are formed, they can propagate in the retrograde as well as in the antegrade direction, thereby interrupting proximal wavefronts.

Another significant finding of this study was that during normal longitudinal conduction, the extracellular corpus slow-wave amplitudes were substantially reduced in gastroparesis compared to those in normal subjects evaluated by equivalent methods (mean 170 vs 250 μV [16]). Extracellular amplitudes are influenced by several factors, including electrode size and design, tissue resistance, conduction direction and velocity [34], however, these factors were controlled for this comparison, and the longitudinal conduction velocity was comparable (2.9 mm s^{-1} vs 3.0 mm s^{-1} in the normal subjects [16]). Reduced current density output may be a consequence of ICC depletion [29], and could contribute to weakened contractions. However, a role for other factors potentially influencing extracellular amplitudes should also be considered, such as the presence of fibrosis.

No clear relationship has yet been established between gastric electrical abnormalities, the symptoms of gastroparesis, and gastric emptying [7,9,35]. Previous studies addressing these relationships have been hindered by low resolution recordings. Antral motility is reduced in gastroparesis [36], and the abnormalities described in this study could be contributory, because uncoupling, wavefront collisions and retrograde propagation must impair motility. However, other mechanisms of hypomotility are also known to be significant in gastroparesis, such as extrinsic neuropathy, impaired neurotransmission, and smooth muscle atrophy [1].

Our results underscore the limitations of EGG for reliably detecting electrical abnormalities, although the method can be useful in detecting abnormalities of frequency and rhythm when present [9,10,37]. The methods applied here could potentially help to improve EGG in future, by unravelling more specific far-field signatures through simultaneous HR-EGG or modeling studies [38]. Perhaps most significantly, HR mapping itself could become a powerful complimentary or alternative tool to EGG, if a less invasive approach could be achieved.

The results here may be applicable to other disorders. For example, EGG irregularities have been detected in more than 30% of functional dyspepsia patients [35,39], potentially encompassing some of the specific abnormalities described here. The results could also inform new treatments; for example, gastric pacing can revert dysrhythmias [40], and could perhaps be better implemented if HR mapping was used as a guide, as occurs in cardiology [41].

Bayguinov et al recently questioned the reliability of GI extracellular recordings, claiming routine contamination by motion artifacts based on in-vitro mouse recordings [42]. Motion suppression is not feasible in clinical studies, however, the signals in this study were strongly indicative of true bioelectrical data. As recently reviewed elsewhere, an extensive literature of theoretical and experimental data supports the veracity of GI extracellular electrical potentials, which directly accord with the biophysics of membrane potentials, and not with movement artifacts [43].

New analysis methods and software were employed in this study. The accuracy of these methods have been validated, and their use greatly improved the efficiency of HR analyses[18,20,21,23]. The reliability of the results was further assured by a careful manual

review. As discussed above, the present study was conducted after general anesthesia. However, no abnormalities were observed in any of 12 normal subjects recently mapped under similar conditions [16], suggesting that experimental conditions were unlikely to have influenced the results. Awake human studies using HR mapping would be highly desirable in the future, if technical advances could allow it. Such studies would enable symptom correlation, as well as monitoring of post-prandial activity.

Supplementary Material

Refer to Web version on PubMed Central for supplementary material.

Acknowledgments

We thank the clinical research and operating room staff at UMMC, Cheryl Bernard of the Mayo Clinic, and Dr. Rita Yassi and Mr. Nira Paskaranandavadivel for invaluable support.

Grant Support:

This work was supported by the NZ Health Research Council (HRC) and the NIH (R01 DK64775, U01DK074007, U01DK074008). GOG was funded by the American Neurogastroenterology & Motility Society (ANMS).

Abbreviations Used

EGG	Electrogastrography
GEMS	Gastrointestinal Electrical Mapping Suite
HR	High-resolution
ICC	Interstitial cells of Cajal
TSS	Total Symptom Severity Score
UMMC	University of Mississippi Medical Center

References

1. Kashyap P, Farrugia G. Diabetic gastroparesis: what we have learned and had to unlearn in the past 5 years. Gut. 2010; 59:1716–1726. [PubMed: 20871131]
2. Grover M, Farrugia G, Lurken MS, et al. Cellular changes in diabetic and idiopathic gastroparesis. Gastroenterology. 2011; 140:1575–85. e8. [PubMed: 21300066]
3. Faussone-Pellegrini MS, Grover M, Pasricha P, et al. Ultrastructural differences between diabetic and idiopathic gastroparesis: The NIDDK gastroparesis clinical research consortium (GpCRC). J Cell Mol Med. 2011 Ahead of Press.
4. Farrugia G. Interstitial cells of Cajal in health and disease. Neurogastroenterol Motil. 2008; 20:54–63. [PubMed: 18402642]
5. Ordog T. Interstitial cells of Cajal in diabetic gastroenteropathy. Neurogastroenterol Motil. 2008; 20:8–18. [PubMed: 18173559]
6. Lin Z, Sarosiek I, Forster J, et al. Association of the status of interstitial cells of Cajal and electrogastrogram parameters, gastric emptying and symptoms in patients with gastroparesis. Neurogastroenterol Motil. 2010; 22:56–61. e10. [PubMed: 19614868]
7. Chen JD, Lin Z, Pan J, et al. Abnormal gastric myoelectrical activity and delayed gastric emptying in patients with symptoms suggestive of gastroparesis. Dig Dis Sci. 1996; 41:1538–1545. [PubMed: 8769276]
8. Bortolotti M, Sarti P, Barara L, et al. Gastric myoelectrical activity in patients with chronic idiopathic gastroparesis. J Gastroint Motil. 1990; 2:104–108.

9. Parkman HP, Hasler WL, Barnett JL, et al. Electrogastrography: a document prepared by the gastric section of the American Motility Society Clinical GI Motility Testing Task Force. Neurogastroenterol Motil. 2003; 2003:89–102. [PubMed: 12680908]
10. Koch KL. The electrifying stomach. Neurogastroenterol Motil. 2011; 23:815–818. [PubMed: 21838727]
11. Lammers WJEP, Ver Donck L, Stephen B, et al. Focal activities and re-entrant propagations as mechanisms of gastric tachyarrhythmias. Gastroenterology. 2008; 135:1601–1611. [PubMed: 18713627]
12. O'Grady G, Egbuji JU, Du P, et al. High-resolution spatial analysis of slow-wave initiation and conduction in porcine gastric dysrhythmia. Neurogastroenterol Motil. 2011; 23:e345–55. [PubMed: 21714831]
13. Abell TL, Camilleri M, Donohoe K, et al. Consensus recommendations for gastric emptying scintigraphy: a joint report of the American Neurogastroenterology and Motility Society and the Society of Nuclear Medicine. Am J Gastroenterol. 2008; 103:753–763. [PubMed: 18028513]
14. Egbuji JU, O'Grady G, Du P, et al. Origin, propagation and regional characteristics of porcine gastric slow-wave activity determined by high-resolution mapping. Neurogastroenterol Motil. 2010; 22:e292–300. [PubMed: 20618830]
15. Lammers WJ, Ver Donck L, Stephen B, et al. Origin and propagation of the slow-wave in the canine stomach: the outlines of a gastric conduction system. Am J Physiol Gastrointest Liver Physiol. 2009; 296:1200–1210.
16. O'Grady G, Du P, Cheng LK, et al. The origin and propagation of human gastric slow-wave activity defined by high-resolution mapping. Am J Physiol Gastrointest Liver Physiol. 2010; 299:585–592.
17. Du P, O'Grady G, Egbuji JU, et al. High-resolution mapping of in vivo gastrointestinal slow-wave activity using flexible printed circuit board electrodes: methodology and validation. Ann Biomed Eng. 2009; 37:839–846. [PubMed: 19224368]
18. Yassi R, O'Grady G, Paskaranandavadivel N, et al. The Gastrointestinal Electrical Mapping Suite (GEMS): Software for analyzing and visualizing high-resolution (multi-electrode) recordings in spatiotemporal detail. BMC Gastroenterol. 2012 In Press. doi to follow.
19. Paskaranandavadivel N, Cheng LK, Du P, et al. Improved signal processing techniques for the analysis of high resolution serosal slow-wave activity in the stomach. Conf Proc IEEE Eng Med Biol Soc. 2011:1737–1740. [PubMed: 22254662]
20. Erickson JC, O'Grady G, Du P, et al. Falling-edge, variable threshold (FEVT) method for the automated detection of gastric slow-wave events in serosal high-resolution electrical recordings. Ann Biomed Eng. 2010; 38:1511–1529. [PubMed: 20024624]
21. Erickson JC, O'Grady G, Du P, et al. Automated cycle partitioning and visualization of high-resolution activation time maps of gastric slow-wave recordings: the Region Growing Using Polynomial Surface-estimate stabilization (REGROUPS) Algorithm. Ann Biomed Eng. 2011; 39:469–483. [PubMed: 20927594]
23. Paskaranandavadivel N, O'Grady G, Du P, et al. An improved method for the estimation and visualization of velocity fields from gastric high-resolution electrical mapping. IEEE Trans Biomed Eng. 2012; 59:882–889. [PubMed: 22207635]
22. Potse M, Linnenbank AC, Grimbergen CA. Automated generation of isochronal maps in the presence of activation block. Int J Bioelectromagnetism. 2002; 4:115–116.
24. Du P, O'Grady G, Paskaranandavadivel N, et al. Quantification of velocity anisotropy during gastric electrical arrhythmia. Conf Proc IEEE Eng Med Biol Soc. 2011:4402–4405. [PubMed: 22255315]
25. Chen, JD.; Lin, Z.; Yin, Y. Electrogastrography. In: Parkman, HP.; McCallum, RW.; Rao, SC., editors. GI Motility Testing: A Laboratory and Office Handbook. SLACK Incorporated; Thorofare, NJ: 2011. p. 81-92.
26. Owyang C, Hasler WL. Physiology and pathophysiology of the interstitial cells of Cajal: from bench to bedside. VI. Pathogenesis and therapeutic approaches to human gastric dysrhythmias. Am J Physiol Gastrointest Liver Physiol. 2002; 283:G8–15. [PubMed: 12065286]

27. Jebbink RJ, Samsom M, Bruijs PP, et al. Hyperglycemia induces abnormalities of gastric myoelectrical activity in patients with type I diabetes mellitus. Gastroenterology. 1994; 107:1390–1397. [PubMed: 7926503]
28. Grover M, Bernard CE, Pasricha PJ, et al. Clinical-histological associations in gastroparesis: results from the Gastroparesis Clinical Research Consortium. Neurogastroenterol Motil. 2012 On-line Ahead of Press [doi to follow].
29. Du P, O'Grady G, Gibbons SJ, et al. Tissue-specific mathematical models of slow-wave entrainment in wild-type and 5-HT2B knockout mice with altered interstitial cell of Cajal networks. Biophys J. 2010; 98:1772–1781. [PubMed: 20441740]
30. Munoz, V.; Zlochiver, S.; Jalife, J. Fibrosis and Fibroblast Infiltration: An Active Structural Substrate for Altered Propagation and Spontaneous Tachyarrhythmias. In: Zipes, DP.; Jalife, J., editors. Cardiac Electrophysiology, From Cell to Bedside. Saunders Elsevier; Philadelphia: 2009. p. 215-221.
31. Coleski R, Hasler WL. Directed endoscopic mucosal mapping of normal and dysrhythmic gastric slow-waves in healthy humans. Neurogastroenterol Motil. 2004; 16:557–565. [PubMed: 15500512]
32. O'Grady G, Du P, Egbuji JU, et al. A novel laparoscopic device for measuring gastrointestinal slow-wave activity. Surg Endosc. 2009; 23:2842–2848. [PubMed: 19466491]
33. Hirst GD, Garcia-Londono AP, Edwards FR. Propagation of slow-waves in the guinea-pig gastric antrum. J Physiol. 2006; 571:165–177. [PubMed: 16357017]
34. O'Grady G, Du P, Paskaranandavadivel N, et al. Rapid high-amplitude circumferential slow-wave conduction during normal gastric pacemaking and dysrhythmia. Neurogastroenterol Motil. 2012 In press: [doi to follow].
35. Sha W, Pasricha PJ, Chen JD. Rhythmic and spatial abnormalities of gastric slow-waves in patients with functional dyspepsia. J Clin Gastroenterol. 2009; 43:123–129. [PubMed: 18719512]
36. Kloetzer L, Chey WD, McCallum RW, et al. Motility of the antroduodenum in healthy and gastroparetics characterized by wireless motility capsule. Neurogastroenterol Motil. 2010; 22:527–33. e117. [PubMed: 20122128]
37. Smout AJPM, Van der schee EJ, Grashuis JL. What is measured in electrogastrography? Dig Dis Sci. 1980; 25:179–187. [PubMed: 7371462]
38. Du P, O'Grady G, Cheng LK, et al. A multi-scale model of the electrophysiological basis of the human electrogastrogram. Biophys J. 2010; 99:2784–2792. [PubMed: 21044575]
39. Leahy A, Besherdas K, Clayman C, et al. Abnormalities of the electrogastrogram in functional gastrointestinal disorders. Am J Gastroenterol. 1999; 94:1023–1028. [PubMed: 10201477]
40. McCallum RW, Chen JD, Lin Z, et al. Gastric pacing improves emptying and symptoms in patients with gastroparesis. Gastroenterology. 1998; 114:456–461. [PubMed: 9496935]
41. O'Grady G, Du P, Lammers WJ, et al. High-resolution entrainment mapping for gastric pacing: a new analytic tool. Am J Physiol Gastrointest Liver Physiol. 2010; 298:314–321.
42. Bayguinov O, Hennig GW, Sanders KM. Movement artifacts may contaminate extracellular electrical recordings from GI muscles. Neurogastroenterol Motil. 2011; 23:1029–e498. [PubMed: 21951699]
43. O'Grady G. Gastrointestinal extracellular electrical recordings: fact or artifact? Neurogastroenterol Motil. 2012; 24:1–6.

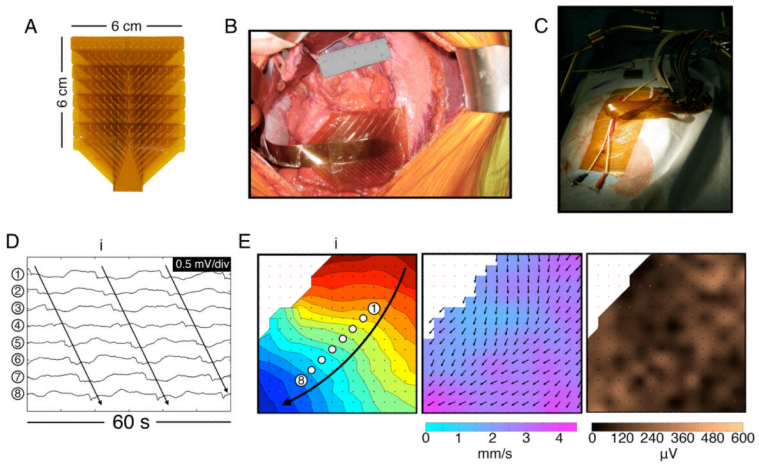

Figure 1.

HR mapping methods. **A**. Flexible PCB array (16×16 electrodes at 4 mm spacing). **B**. Photo of the array placed on the corpus-antrum border. **C**. During mapping, the wound edges were approximated and cables fixed to a retractor. **D**. Electrograms from 8 channels from the positions indicated in *(E)* (frequency 3.2 ± 0.1 SD c/min) (Patient ID#3 in Suppl. Table 2). **E**. *Left*: isochronal activation map of the wavefront *(i)* indicated in (D), showing normal propagation. Each dot represents an electrode, and each color band shows the area of slow-wave propagation per 2 s (the 'isochronal interval'). An animation sequence of this data is presented in Figure1.wmv. *Middle*: Velocity field map of the same wavefront *(i)*, showing the speed (color spectrum) and direction (arrows) of the wavefront at each point on the array. Propagation is faster nearer the greater curvature [16]. *Right*: Amplitude map of the same wavefront *(i)*.

Figure 2.
Comparison of gastric circular muscle ICC counts between the gastroparesis patients and matched controls (mean difference 3.2 bodies/field [CI: 2.1, 4.2]; P<0.0001).

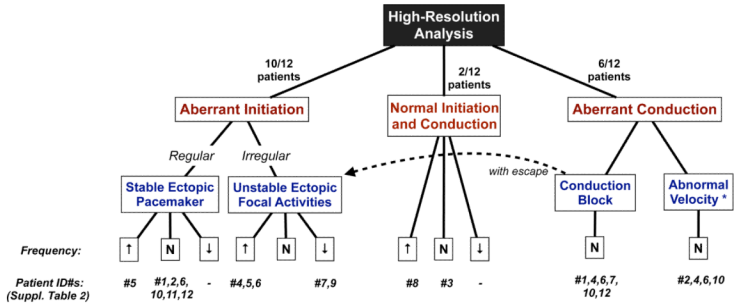

Figure 3.

Classification of slow-wave abnormalities in this study. Patients #1-8 had diabetic gastroparesis and patients #9-12 idiopathic; no differences in dysrhythmic patterns were apparent between these groups in this cohort. *Refers to the velocity of longitudinal conduction components only.

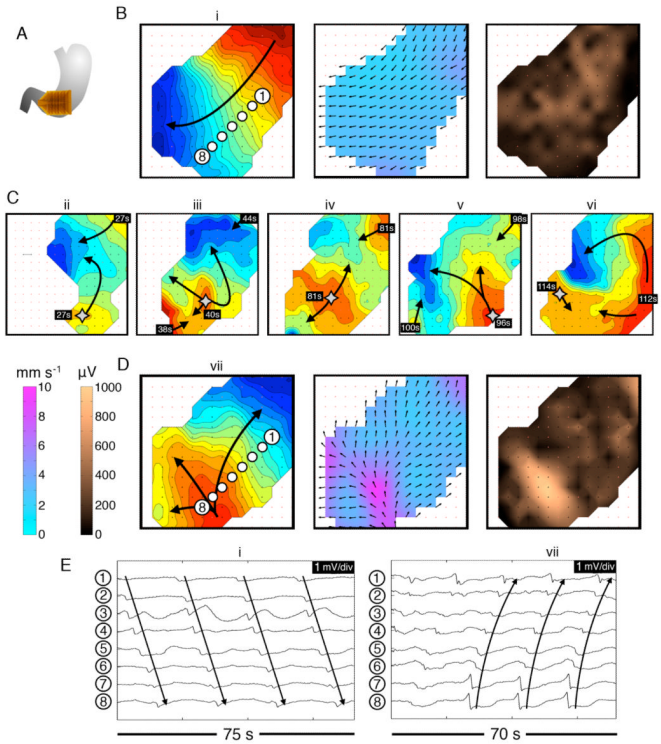

Figure 4.

Abnormal slow-wave initiation: unstable focal events and stable ectopic pacemaking; examples from diabetic gastroparesis (ID#5). Isochronal intervals = 1 s. **A**. Position diagram. **B**. Normal activity was initially mapped for 280 s (freq. 3.3 ± 0.1 SD c/min). Isochrone, velocity and amplitude maps are shown for example wave (*i*) (see also animation Figure4i.wmv). **C**. An irregular tachygastria followed, due to unstable ectopic events arising at multiple locations (stars; duration ~200 s). Isochronal maps of 5 representative cycles (*ii-vi*) demonstrate chaotic tissue activation and wave collisions, resulting in a range or frequencies across the mapped field (median 3.7 c/min; range: 1.4 – 5.7). Time stamps are referenced to the accompanying animation (Figure4ii.wmv). **D**. Regular tachygastria followed, due to stable ectopic activity (freq. 4.0 ± 0.05 SD c/min), with organized retrograde propagation occurring until the end of the recording period. Isochrone, velocity and amplitude maps are shown for example wave (*vii*) (see also animation Figure 4iii.wmv). During aberrant initiation, circumferential slow-wave propagation emerged, and was faster than normal longitudinal conduction (6.4 ± 2.0 SD *vs* 2.8 ± 0.7 SD mm s^{-1}; P<0.001), with higher amplitudes (595 ± 225 SD *vs* 240 ± 150 SD μV; P<0.001). **E**. Representative electrograms from waves (*i)* and (*vii)*, from the channels shown in *B,D*.

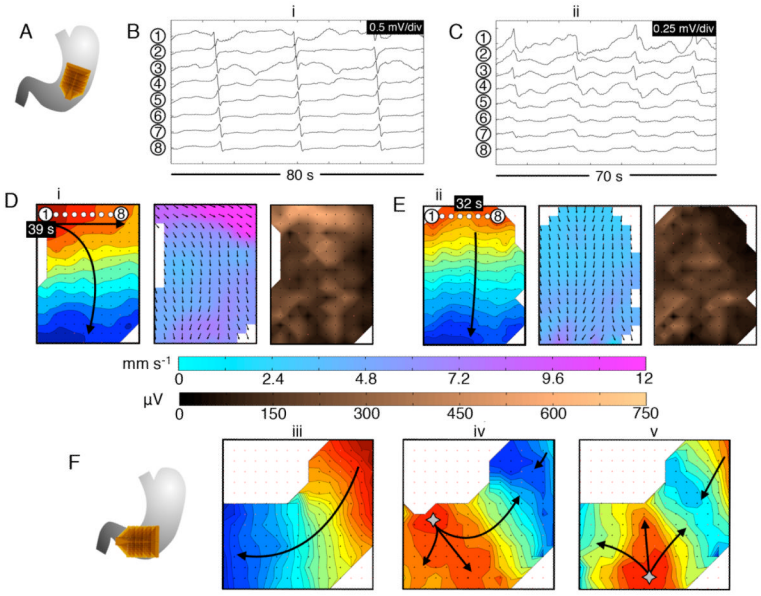

Figure 5.

Abnormal slow-wave initiation at low frequency. **A**. Position diagram relating to (B-E); diabetic gastroparesis (ID#1). **B,D**. Stable ectopic pacemaking originated near the lesser curvature of the mid-corpus, at a slightly lower than normal frequency (2.4 ± 0.05 SD c/min). Isochronal (intervals = 1s), velocity and amplitude maps are shown for typical wave *(i)* (see also animation Figure5i.wmv). **C,E**. The ectopic pacemaker was transient, being followed by activity of normal pattern and frequency (3.0 ± 0.05 SD c/min). Maps are shown for representative wave *(ii)* (see also animation Figure5ii.wmv). During ectopic pacemaking, circumferential slow-wave propagation occurred, and was faster than normal longitudinal conduction (10.7 ± 6.2 SD *vs* 3.3 ± 1.5 SD mm s^{-1}; P<0.001), with higher amplitudes (270 ± 155 SD *vs* 80 ± 40 SD μV; P<0.001). The time stamps are marked relative to the animations. **F**. A further example of propagation patterns during bradygastric activity, mapped at the corpus-antrum border, in idiopathic gastroparesis (ID#9). Normal activity (frequency 2.9 ± 0.1 SD c/min); e.g. wave (*iii*), was followed by a period of unstable ectopic focal events at a lower than normal frequency (2.2 ± 0.5 SD); waves (*iv, v*), which caused retrograde-propagating wavefronts that collided with proximal activities.

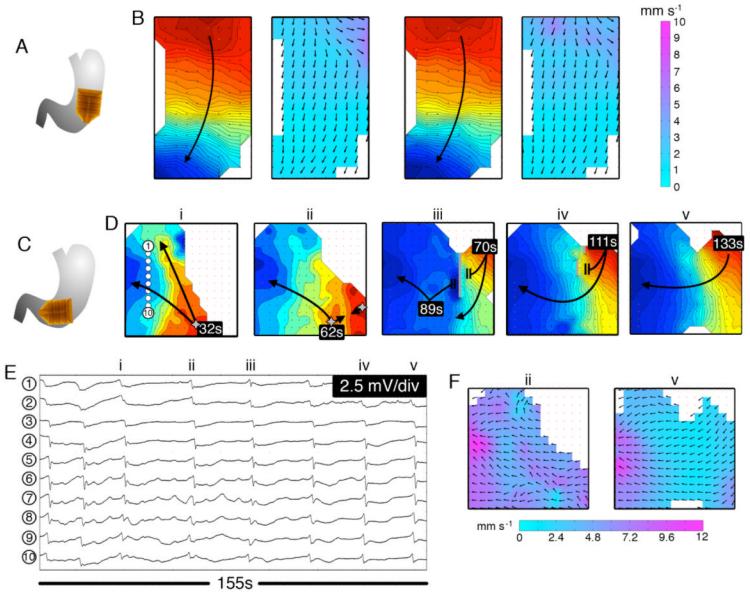

Figure 6.

Abnormalities of slow-wave conduction. **A**. Position diagram (diabetic gastroparesis; ID#4), pertaining to (B,C). **B**. Isochronal maps (intervals = 1 s) and velocity maps of two consecutive wavefronts, demonstrating a marked, fixed reduction in corpus longitudinal conduction velocity in the distal field (<1 mm s^{-1}). Animation Figure6i.wmv demonstrates how the reduced velocity caused wavefront crowding (wave-spacing <2 cm; normally 5-6 cm [16]); frequency = 3.5 ± 0.1 SD mm s^{-1}. **C**. Position diagram (diabetic gastroparesis; ID#4), pertaining to (D-F). **D**. Isochronal maps (*i-v)* show representative wavefronts (intervals = 1 s; refer also animation Figure 6ii.wmv), with example electrograms shown in **(E)** (channel positions indicated in map (*i*). A series of abnormal initiation events repeatedly occurred in the lower half of the mapped field (waves *i-iii*). Further mapping (waves *iii-v* and animation) revealed a fixed area of marked reduction in corpus conduction velocity in the right mapped field (crowded isochrones), accompanied by intermittent conduction blocks (grey bars). Abnormal initiation occurred immediately distal to the region of aberrant conduction, and was often related to delayed excitation (Figure 6ii.wmv). **F**. Velocity maps are shown for waves (*ii)* and (*v)*, demonstrating the rapid circumferential conduction during aberrant initiation (*ii*) and the markedly reduced longitudinal conduction velocity (<1 mm s^{-1}) (*v*).